Engineering Failure Analysis 191 (2026) 110776

Contents lists available at ScienceDirect

Engineering Failure Analysis

journal homepage: www.elsevier.com/locate/engfailanal

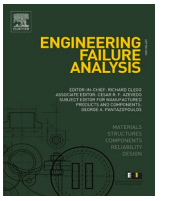

Dynamic failure mechanism and liability assessment of mine tremor induced rock bursts

Jiang He [a,b,c,1], Guanzhong Qiu [a,b,c,*], Linming Dou [a,b,c], Siyuan Gong [a,b,c], Andrew Pan [d], Zonglong Mu [a,b,c]

[a] School of Mines, China University of Mining and Technology, Xuzhou 221116, China
[b] Key Laboratory of Deep Coal Resource Mining, Ministry of Education of China, China University of Mining and Technology, Xuzhou, Jiangsu 221116, China
[c] Jiangsu Engineering Laboratory of Mine Earthquake Monitoring and Prevention, China University of Mining and Technology, Xuzhou, Jiangsu 221116, China
[d] Faculty of Applied Science and Engineering, University of Toronto, Toronto, Ontario M5S 1A4, Canada

ARTICLE INFO

Keywords:
Rock burst
Mine tremor
Dynamic loading
Strain rate dependency
Rock burst liability
Energy evolution

ABSTRACT

Rock bursts represent one of the most severe hazards in underground coal mining, making a comprehensive understanding of their underlying mechanisms paramount. While these events are frequently triggered by dynamic loads from mine tremors, their specific dynamic mechanisms and corresponding evaluation metrics remain inadequately defined. This study employs a comprehensive methodology—combining field statistical analysis, waveform spectrum analysis, dynamic loading experiments (across strain rates from 1.0×10^{-5} to $1.0 \times 10^{-2} s^{-1}$), and fracture mechanics theory—to elucidate the failure mechanisms and dynamic rock burst liability (RBL) of coal under tremor-induced dynamic loading. Field monitoring data confirms that over 83.1% of rock bursts are tremor-induced, a finding further substantiated by waveform spectrum characteristics. Our experimental results reveal an exponential correlation between energy accumulation and loading strain rate. Notably, elevated strain rates accelerate the transition from static to dynamic brittle failure, accompanied by a marked surge in acoustic emission rates. A critical finding is that while RBL intensifies with increasing strain rate, the traditional bursting energy index (KE) paradoxically decreases, rendering KE invalid for dynamic RBL assessment. Consequently, total energy accumulation and its rate of change are proposed as more robust and reliable indicators. From a mechanistic perspective, the time-varying nature of principal stress direction and magnitude under dynamic loading drives instantaneous, large-scale crack propagation across multiple directions, culminating in the violent destruction of the coal mass. The proposed energy assessment framework and mechanism provide professional personnel with practical guidance and references for optimizing microseismic monitoring and preventing impact ground pressure.

1. Introduction

Rock burst is a major dynamic disaster that poses a threat to safe coal mining [1]. Numerous countries including Poland [2], the

* Corresponding author at: School of Mines, China University of Mining and Technology, No.1 Daxue Rd, Xuzhou 221116, China.
E-mail address: 15804046808@163.com (G. Qiu).
[1] **First Author (ORCID):** https://orcid.org/0000-0001-9315-9288.

https://doi.org/10.1016/j.engfailanal.2026.110776
Received 13 January 2026; Received in revised form 1 March 2026; Accepted 16 March 2026
Available online 22 March 2026

Czech Republic [3], China [4,5], the USA (Christopher 2016, [6], Australia [7], Germany, Russia, and South Africa [8–10] are susceptible to this type of disaster. In China alone, more than 200 coal mines are at risk of rock bursts, with incidents occurring every year [4]. Despite significant progress in rock burst prevention and control after long-term research, China has experienced several severe rock burst disasters in the past five years, leading to 45 fatalities [5]. Consequently, rock burst has emerged as a research focus for coal mine disaster prevention in recent years.

Rock burst is a dynamic instability failure caused by the superposition of static stress concentration and dynamic stress disturbance to reach the critical load of rock burst [11,12]. The conceptual model for rock burst can be presented as Eq. (1).

$$\sigma_s + \sigma_d \geqslant \sigma_c \tag{1}$$

Where σ_s is the static stress of surroundings, σ_d is the dynamic stress disturbance caused by seismic waves, and σ_c is the critical stress condition under which a rock burst occurs. Therefore, an assessment and prediction of rock burst risk can be conducted from a stress analysis of mining areas utilizing the intensity of seismic stress wave disturbance.

Rock burst is a type of failure that occurs in rocks due to the combination of static stress concentration and dynamic stress disturbance. This phenomenon is explained by the superposition theory of dynamic and static loads [11,12]. The critical load required for rock burst to occur can be represented by Eq. (1), which takes into account the static stress of the surroundings, the dynamic stress disturbance caused by seismic waves, and the critical stress condition. To assess and predict the risk of rock burst, stress analysis of mining areas can be carried out by analyzing the intensity of seismic stress wave disturbance.

In order to determine the likelihood of a rock burst, Eq. (1) takes into account three factors: the static stress state of the coal body, the strength of the mine's seismic load disturbance, and the critical load of the rock burst. A thorough analysis of all three factors is necessary for accurate prediction and monitoring of the risk of a rock burst.

Rock burst initiation is primarily caused by high-stress levels [13]. Underground mining stress in coal mines is influenced by various factors such as mining depth, hard roof, fault, fold structure, coal seam thickness, structural variation, coal pillars, roadway bottom coal, and mining layout. Numerous studies have focused on understanding the impact of different factors on stress and how they affect the occurrence of rock bursts. For instance, Pu Wang et al. [14] explored the rock burst disaster caused by stress concentration in the hard thick roof area, while Zhenlei [15,16] studied the mechanism of rock burst caused by instability due to stress concentration of fault coal pillar. He and Dou [17] investigated the law of rock burst induced by horizontal stress in the wall of a coal seam roadway. Due to the complexity of the influencing factors of rock bursts, research in this area focuses on understanding the impact of specific main control factors on rock bursts and their targeted prevention and control.

Aside from stress, other factors such as mining disturbances, movement of rock strata, and other mining vibration loads are also being examined for their influence on mine tremors. Current research on mine tremors focuses on understanding their focal mechanism [18,19], the time–space intensity variation law [20,21], and developing analysis indicators for predicting or warning of rock burst risk based on monitoring data [22,23]. Laboratory tests are also being conducted to study the dynamic capacity of energy-absorbing rock bolts under varying impact energy and strain rates [24,25], particularly on the effect of mine tremor load on the roadway [26]. Although research on mine tremor activity near the appearance before and after a rock burst has been conducted to find sensitive precursor indicators of the mine tremor activity law, there has been no specific study on how to induce a rock burst, nor has it been clearly proven that mining tremors can cause a rock burst.

The goal of studying rock burst is to better understand its mechanism and risk and to find effective ways to prevent and control it. As a significant topic in mining ground pressure control research, it is crucial to evaluate the likelihood of a rock burst in order to prevent it. This is done by analyzing and monitoring the stress state and mining vibration load pattern. The determination of the critical load is key to assessing the risk of rock burst, which is related to the inherent properties of coal. The RBL test method is primarily used to evaluate the impact of coal's mechanical properties on the risk of rock burst [27]. The RBL of coal serves as an index for assessing the possibility of a rock burst in a coal mine. The predisposition to rock burst is a physical precondition for its occurrence in coal mining.

A. Kidybiński [27] proposed three indices for evaluating the RBL of coal in studying rock bursts in Poland. In China, the RBL is established by assessing four indices: UCS, K_E, W_{ET}, and D_T [28]. These indices are obtained from static loading tests conducted under specific conditions and at low strain rates. However, recent studies have shown that rock bursts occur due to dynamic destabilization of the coal masses caused by dynamic disturbance under high stress [29–33]. Most existing studies on the mechanical properties of coal involve testing its static mechanical properties at low strain rates (lower than 10^{-5} s^{-1}). However, the research on mining seismicity in coal mines has shown that medium to higher strain rates (10^{-1} s^{-1}) can be applied to coal and rock, due to the dynamic disturbance caused by mine tremors [34]. Studies have also revealed a strong correlation between the mechanical properties of coal and strain rate [35,36]. Therefore, it is essential to study the mechanical properties of coal under the effect of dynamic loads at medium and high strain rates to accurately evaluate the RBL of coal.

Recent research on the mine micro-seismic monitoring system has provided some insights into the causes of rock bursts. It is still unclear whether the mine seismic event is caused by the vibration generated by the rock burst itself or the mine tremor event that induced the rock burst. The statistics and waveforms of rock bursts were analyzed to prove that mine tremors can indeed cause them. The characteristics of the dynamic load induced by mine tremors were examined to understand how it affects the evolution of coal mechanical properties and RBL under similar loading strains. After thorough analysis and discussion of the test results, the evolution law of dynamic RBL of coal and the law of induced burst fracturing under the action of mine tremor load were presented. These findings can serve as a valuable reference for future research on the mechanism of rock bursts and risk assessments.

2. Evidence of mine tremor inducing rock burst

2.1. Statistical analysis of rock bursts

Numerous scholars posit that rock bursts are the result of a combination of dynamic and static loads [4,37]. Dynamic loads stem from mining-induced seismic activity, while static loads originate from the surrounding rocks. However, due to the sudden and unpredictable nature of rock bursts, establishing a clear link between the two is challenging. To address this issue, the present study employs statistical analysis to explore the correlation between dynamic loads caused by mining-induced seismic activity and rock bursts.

Seismic activity is a common occurrence in coal mining operations [20,38], where seismic waves propagate through the coal and rock mass, generating dynamic loads that impact the stability of the surrounding environment. Due to the rapid and dynamic nature of this seismic activity, studying its impact on rock bursts can prove to be challenging. Researchers have therefore relied heavily on analyzing micro-seismic monitoring results at mining sites to investigate this topic.

Fig. 1 depicts the production process of the working face during 474 severe rock burst disasters in Huating mining area of Gansu, Yima mining area of Henan, and Hegang mining area of Heilongjiang provinces in China. Fig. 1 illustrates that 67.9% of rock bursts occur during the mining process of the working face, while 18.1% occur during roadway excavation. The proportion of rock bursts during the strong disturbance period of mining and excavation reaches 86.0%. Although mining seismic activity may occur during other periods, it is relatively weak when compared to the mining period. As such, it can be inferred that there exists a close relationship between rock bursts and the induced disturbance of mining seismic dynamic load, based on the mining process when rock bursts occur.

Fig. 2 delineates the minimum distance between the location of the seismic source monitored by the micro-seismic monitoring system and the area of rock burst damage. The graph illustrates that the distance from the source to the damaged area is a minimum of 50–100 m, comprising 28.5% of the total distance. The distance exceeding 100 m accounts for 54.6%, while the total distance exceeding 50 m is 83.1%, with a proportion of less than 50 m being only 16.9%. As the micro-seismic monitoring system utilized in coal mines demonstrates an error of less than 50 m for seismic sources [39], especially for high-energy mine seismicity that occurs during a rock burst, where the waveform is relatively clear and the position calculating error is comparably lower. Based on this analysis, it can be concluded that at least 83.1% of the seismic sources are located in different regions from the rock burst. This suggests that rock bursts are triggered by seismic activity. These statistics indicate that the vast majority of rock bursts are influenced by dynamic loads induced by mining seismicity.

2.2. A case study of seismicity-inducing rock burst

On February 20, 2020, a rock burst event transpired in the roadway section located in front of the 2305 working face of Shandong Xinjulong Coal Mine. The area of damage caused by the rock burst is depicted in Fig. 3. Based on the micro-seismic monitoring location, the center of the area affected by the rock burst is approximately 200 m away from the source. The incident caused damage to 486 m of roadway to varying degrees, and the most severe damage resulted in the closure of the roadway. The rock burst caused four fatalities, and the consequences of the disaster were extremely severe.

Within Fig. 4 a, the micro-vibration pickup sensor (S21) was situated 750 m away from the rock burst area and captured the entire seismic waveform during the occurrence of the rock burst. When a mine tremor triggers a rock burst, both the mine tremor and rock burst become sources. The waveforms of these sources are then superimposed, rendering it arduous to differentiate due to their

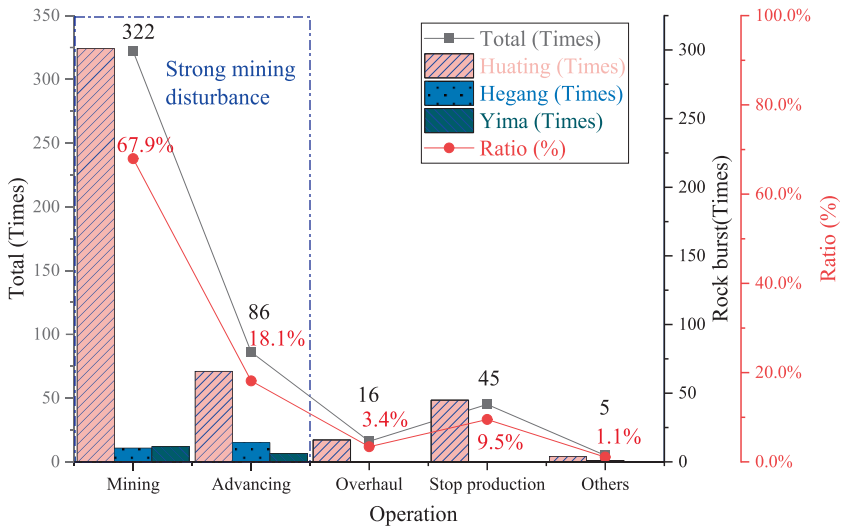

Fig. 1. Statistical relationship between the occurrence time of a rock burst and the mining process.

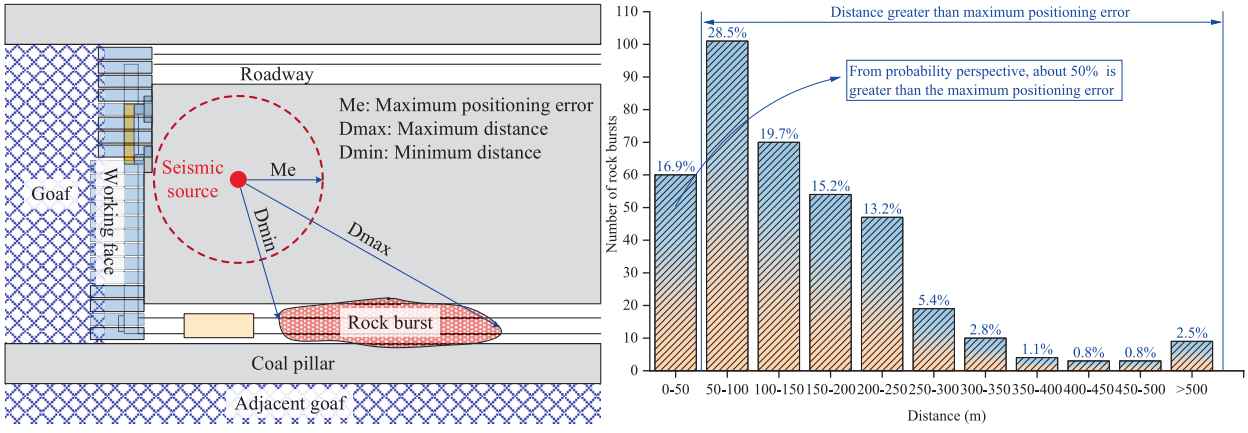

(a) The location of the source and the damaged area

(b) Statistics of minimum distance distribution

Fig. 2. Statistic of the minimum distance between seismic source and destruction zone of rock bursts.

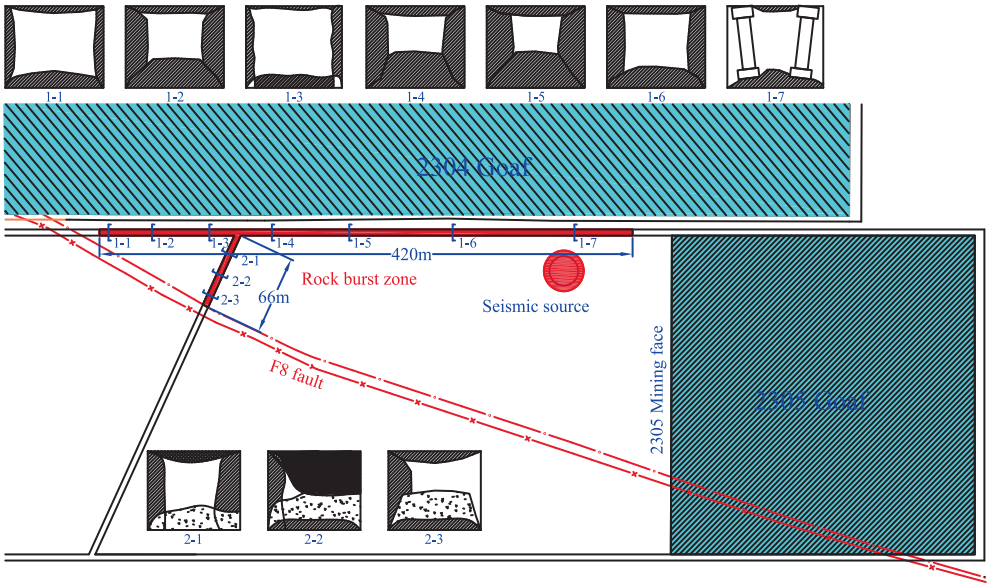

(a) layout of 2.22 rock burst

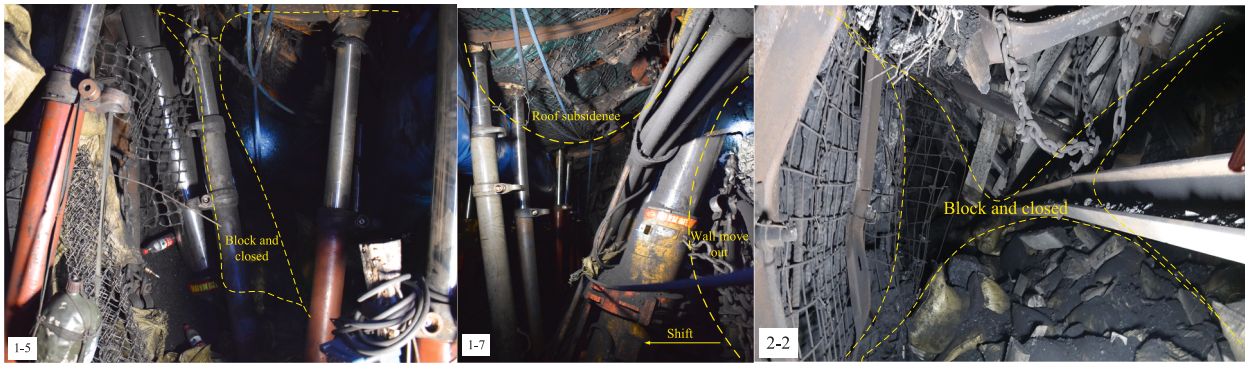

(b) Photos of damaged roadway

Fig. 3. Photos of rock burst taking place in the roadway of 2305S mining face.

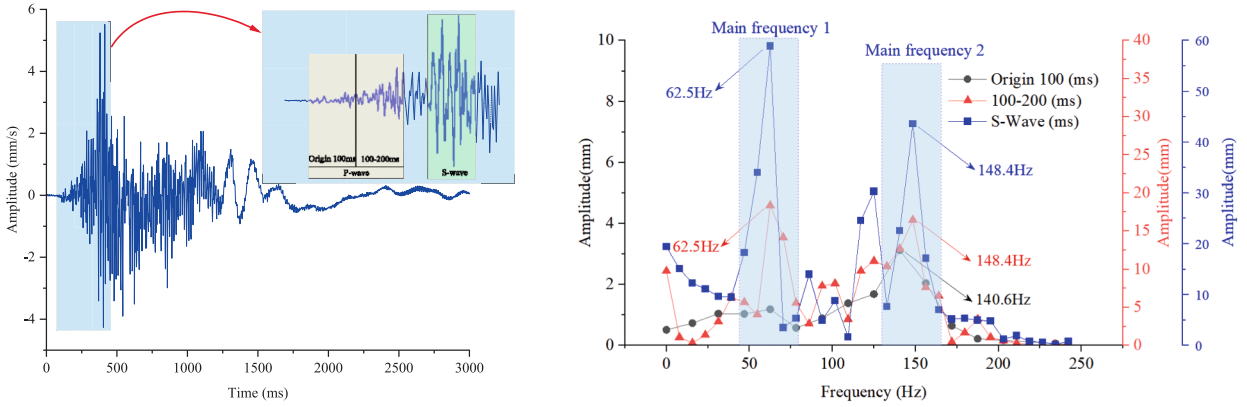

(a) 2020.2.20 rock burst location and waveform

(b) Sectional frequency spectrum analysis

Fig. 4. Frequency spectrum analysis relationship between rock burst and mine tremor.

proximity. However, if the rock burst is the aftermath of damage caused by the mine tremor at the monitored source, the distance disparity between the mine tremor and the wave generated by the rock burst center to the S21 sensor is approximately 400 m. Statistical research has extensively shown that the propagation speed of direct P-waves underground in coal mines is about 4000 m/s. Thus, the time difference between the two tremor direct waves that propagate to the S21 sensor is approximately 100 ms, according to the Brune model [40]. This model approximates the epicenter radius of a mine tremor as:

$$R_0 = \frac{K_c \beta_0}{2\pi f_c} \tag{2}$$

Where, K_c is a constant depending on the source model, equals 2.34; β_0 is the S-wave velocity in the source area; f_c is the corner frequency of either the P or S wave which can be replaced by the main frequency of the wave.

According to Eq. (2), if there are two tremors, the source radii are different, and the main frequencies of the two tremors are also different. Therefore, through spectrum analysis, the main frequency of the seismic wave of S21 original 100 ms is the main frequency of the tremor-induced rock burst, and the subsequent seismic wave includes both the main frequency of the tremor-induced rock burst and the main frequency of the tremor of rock burst.

Perform Fourier transform analysis on the frequency spectrum of S21 waveform segmentation, as shown in Fig. 4 b. Spectrum analysis shows that the main frequency of the original 100 ms waveform is 140.6 Hz. There are two main frequencies of the waveform between 100 ~ 200 ms, namely 148.4 Hz and 62.5 Hz. The waveform spectrum analysis of the S-wave energy release section shows that during the energy release process of rock burst damage, the coal body has a large range of damage, and the frequency components are relatively complex. There are many local main frequencies, but overall, the two frequency components with the highest values are 148.4 Hz and 62.5 Hz. Based on the analysis of the main frequency of the above three section waveforms, it can be concluded that the main frequency of the initial 100 mm waveform is the main frequency of the tremor source inducing the rock burst, which is 140.6 Hz, corresponding to the larger main frequency of 148.4 Hz in the subsequent two section waveforms; The other main frequency of the following two sections of waveform, 62.5 Hz should be the main frequency of the rock burst source. At the same time, it can be seen that the main frequency of the tremor inducing rock burst is higher, and the main frequency of the rock burst is lower, that is, the energy released by the destruction of the rock burst is much greater than that of the tremor inducing rock burst, which is consistent with the occurrence law of rock burst. The frequency spectrum analysis of the waveform shows that the rock burst was induced by the disturbance of the mine tremor dynamic load.

3. Experimental investigation of dynamic mechanical properties

3.1. Necessity and scheme of experiment

Upon analyzing statistical data and frequency spectrums of rock bursts, it becomes apparent that the majority of these occurrences stem from the dynamic load of mine tremors. The strain rate of coal has a significant correlation with its mechanical properties [35,36]. In order to evaluate the risk of rock bursts under specific conditions, it is imperative to study the dynamic characteristics of coal under the strain rate dynamic load that corresponds to mining seismic waves.

RBL which stands for several mechanical parameters that test the dynamic failure of coal samples under specific quasi-static test conditions, is an integral aspect of comprehensively assessing the mechanical properties of rock bursts in coal seams [28,41]. Therefore, it is critical to analyze the changing pattern of RBL of coal by utilizing the dynamic loading that involves equivalent stress fluctuation and strain rate of mine tremors to assess the risk of rock bursts.

According to national standards, the RBL of coal is evaluated using four indices [28,42] as shown in Table 1. The W_{ET} necessitates an approximate *UCS* of coal in advance, and then the index is obtained through a cyclic load test that targets an unloading capacity of

80% of the *UCS*. However, the dynamic strength of coal remains uncertain during loading at high strain rates, and cyclic loading is more challenging to control. Consequently, the correlation between coal's rock burst liability and the applied strain rate was analyzed using the remaining three indices.

3.2. Experiment

3.2.1. Test setup

The highest seismic strain rate recorded in coal mines usually falls between 10^{-3} and $10^{-1}s^{-1}$ [34], which is higher than the strain rate used in RBL testing for coal. The strain rates for various energy levels are presented in Fig. 5. To carry out mechanical testing in this range of strain rates, an electro-hydraulic servo testing machine can be utilized. For conducting uniaxial load tests on standard coal samples at different loading rates, a mechanical test system was employed, utilizing a displacement-controlled loading approach, as illustrated in Fig. 6. The applied strain rate is:

$$\dot{\varepsilon} = \frac{v}{h} \tag{3}$$

Where v represents the displacement loading rate and h is the height of the samples.

The experimental study was conducted to investigate the variations in dynamic impact propensity index under the influence of mine tremor dynamic load strain rate. The loading scheme designed for this study is as follows. The loading displacement were: 0.06, 0.3, 0.6, 1.5, 3, 6, 30, and 60 mm/min. On this basis, it was calculated (from Eq. (3) that the strain rates applied to the standard coal samples were 1.0×10^{-5}, 5.0×10^{-5}, 1.0×10^{-4}, 2.5×10^{-4}, 5.0×10^{-4}, 1.0×10^{-3}, 5.0×10^{-3}, and 1.0×10^{-2} s^{-1}, respectively. Corresponding to various strain rates, convert them into displacement based on the height of the specimen and conduct uniaxial loading tests until the specimen fails.

In order to facilitate the analysis of the coal rock fracture process, during the experiment, an acoustic emission (AE) detection system was used to acquire the AE signals while the loading of the samples. By analyzing the AE event count data, the energy released by micro-cracking was revealed at different strain rates.

The MTS-C64.106 electro-hydraulic servo system for rock dynamic experiments was used as the loading system, and its rated loading capacity, the displacement speed of the actuator, and the maximum cross-head velocity were 1,000 kN, 0.5 to 90 mm/min, and 200 mm/min, respectively. The system has a test precision at the grade used of 0.5 and a displacement resolution of 0.2 μm. In addition, the maximum data acquisition frequency and controlled cyclic frequency are both 1,000 Hz.

The AE data was collected using the integrated PCI-2 AE acquisition system produced by the Physical Acoustics Corporation (USA). Comprising an 18-bit A/D converter, the system has a sampling frequency of up to 40 MHz. The system is mainly composed of a pre-amplifier, a filter circuit, an A/D conversion module, a waveform processing module, and a computer. The AEWin software system is equipped with function for setting sampling parameters, signal acquisition, A/D conversion of signals, data storage and graphic display, spectral analysis, and real-time location display.

As demonstrated in Fig. 6, the AE system collected signals using four sensors during the experiment. With a fixed threshold (35 dB), the AE system was set with a pre-amplification of 40 dB, a sampling rate of 2 MHz, a pre-trigger of 256 μs, and a hit length of 3 k. In addition, the PDT, HDT, and HLT were 50 μs, 200 μs, and 300 μs, respectively.

3.2.2. Sample preparation

The coal was collected from the coal mine with rock burst hazards and machined into samples according to the regulations in

Table 1
Rock burst liability classification according to the Chinese standard (GB/T25217.2–2010,2010).

Coal burst liability indices		D_T/ms	K_E	W_{ET}	*UCS*/MPa
Schematic drawing of calculation		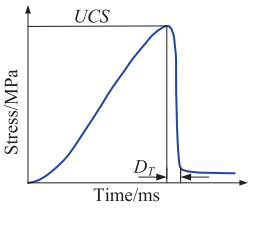	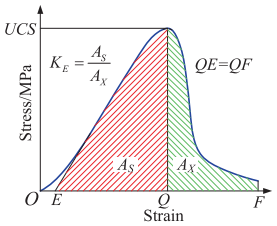	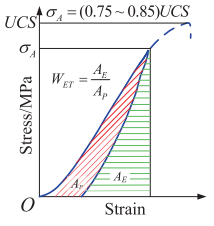	
Standard specimens		Cylindrical specimens with a height of 100 mm and diameter of 50 mm, or cuboid specimens with a height of 100 mm and side length of 50 mm.			
Control mode		Force loading	Displacement loading	Force loading	Force loading
Loading rate		0.5 MPa/s ~ 1.0 MPa/s	0.5×10^{-5}m/s ~ 1.0×10^{-5}m/s	0.5 MPa/s ~ 1.0 MPa/s	0.5 MPa/s ~ 1.0 MPa/s
Classification criteria	None	$D_T > 500$	$K_E < 1.5$	$W_{ET} < 2$	$UCS < 7$
	Weak	$50 < D_T \leq 500$	$1.5 \leq D_T < 5$	$2 \leq W_{ET} < 5$	$7 \leq UCS < 14$
	Strong	$D_T \leq 50$	$D_T \geq 5$	$W_{ET} \geq 5$	$UCS \geq 14$

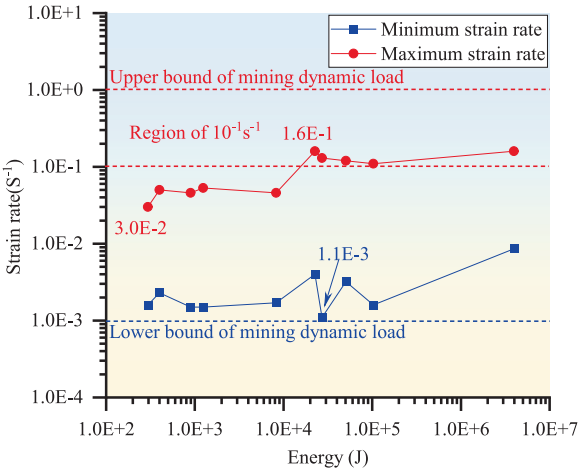

Fig. 5. Statistical results of strain rate range of mine tremors.

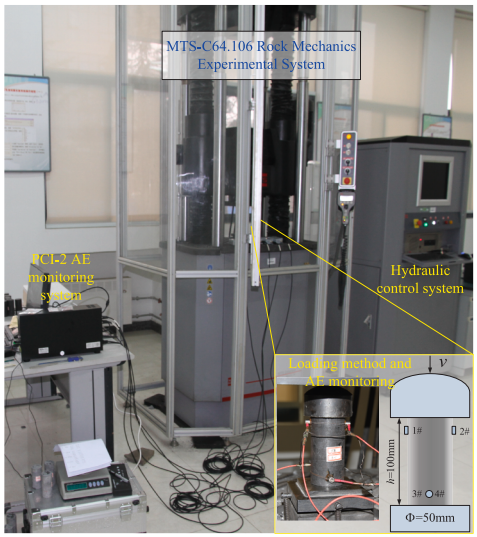

Fig. 6. Loading and test scheme.

Methods for Determining the Physical and Mechanical Properties of Coal and Rock [43]. To begin with, coal cylinders with a diameter of 50 mm were drilled and sawed to coal samples of a height of approximately 100 mm. Then, the two ends of the samples were ground, until they were machined to standard coal samples with the misalignment of the two ends being no larger than 0.05 mm, the diametral deviation of the two ends was within 0.3 mm, and the axial deviation no greater than 0.25°. The parameters of the coal samples, including the size and density, are listed in Table 2.

Table 2
Parameters of the coal samples.

No.	Diameter/mm	Height/mm	Mass/g	Density/(g/cm^3)	Loading rate/(mm/min)
1	49.71	101.47	276.25	1.40	0.06
2	49.80	96.44	256.17	1.36	0.3
3	49.85	101.35	286.52	1.45	0.6
4	49.77	99.20	282.05	1.46	1.5
5	49.97	97.93	298.67	1.55	3
6	49.80	101.91	310.71	1.57	6
7	49.75	96.38	275.59	1.47	30
8	49.79	99.28	328.15	1.67	60

3.3. Result

3.3.1. Mechanical properties under different strain rates

In Table 3, the results of mechanical tests performed on coal samples, including elastic modulus(E) and *UCS* can be found. Fig. 7 displays the correlation between these parameters and the applied strain rates. It is worth noting that both the E and *UCS* of the coal samples exhibited a consistent increase with increasing strain rates. They conform to power function increase. It should be noted that the results of sample 7 shown in Fig. 7 deviate significantly from the data pattern, and the values of this sample were removed from the data fitting. The experimental research results are basically consistent with the experimental research results on rock samples in reference [44], indicating that the rate correlation of mechanical properties of coal is consistent with that of rocks. Based on the rate correlation characteristics demonstrated by the experimental research on the mechanical properties of coal, the strain rate can be adjusted to $1.0 \times 10^{-3}\ s^{-1}$ is used as the critical value to define the dynamic and static loads of coal mines. Based on Fig. 5, it can be seen that the disturbance effect of mining seismic stress waves on coal has reached a state of dynamic load. The disturbance effect of mining seismic on coal needs to consider the influence of the loading strain rate. At this time, the coal and rock impact propensity obtained through static loading testing is not suitable for evaluating the impact risk under mining seismic disturbance actions. It is necessary to test the RBL of coal under the corresponding strain rate of mining seismic to more accurately evaluate the rock burst risk.

3.3.2. Correlation between the RBL and strain rate

Table 4 lists the test results of the index for RBL of the coal samples. Table 4 shows that the K_E gradually decreases with increasing strain rate. According to the national standard, taking K_E into account, the RBL of the coal samples decreases.

With respect to D_T, as the strain rate increases, the D_T of the coal samples decreases from tens of thousands of milliseconds to hundreds of, and even tens of milliseconds. According to the national standard, the grade of RBL is none while the strain rate is lower than 5.11×10^{-4}/s, while it changes from none to strong with the increasing loading strain rate as adjudged from the index of D_T.

Meanwhile, it can be seen from Table 4 and Fig. 7 that the *UCS* of coal increased with increasing loading strain rate. According to the national standard for assessing RBL, the larger the *UCS*, the higher the RBL is. For these coal samples, they showed a weak RBL at strain rates below $9.81 \times 10^{-4}\ s^{-1}$ while showing a strong RBL at strain rates exceeding $9.81 \times 10^{-4}\ s^{-1}$.

An analysis of the above three indices for RBL reveals that the coal samples show growing apparent RBL with increasing loading strain rate according to the *UCS* and the D_T. While the K_E indicates an inverse trend from strong to weak liability with the increasing loading strain rate.

3.3.3. Energy accumulation and dissipation

The energy input by the loading system into the coal samples during loading at different strain rates is displayed in Table 5 and Fig. 8. This involves the relationships of the total, pre-peak, and post-peak energy inputs with the strain rate. With the increasing in strain rate, the pre- and post-peak energy inputs of the loading system to the coal samples grew exponentially. It is worth noting that the energy input curve shows similar characteristics to the curves for *UCS* and elastic modulus. The total, pre-peak, and post-peak energy inputs of the press machine all display an increasing trend with increasing strain rate. These input all grew rapidly, subject to exponential function law with increasing strain rate.

3.3.4. Correlation between failure mode and strain rate

The failure mode of each coal sample is shown in Fig. 9, which reveals that the higher the strain rate, the more serious the damage to the coal samples. The failure modes changed gradually from shear failure to longitudinal splitting failure and eventually burst failure. The broken blocks became gradually smaller and the ejection speed and distance travelled by the ejected blocks both showed a gradually increasing trend. During the experiment, the noise emitted during the failure process became louder with the increase in strain rate. At a low strain rate, the broken blocks were not separated from the matrix of the coal samples. However, as the strain rate increased, the broken blocks were separated from the matrix and the ejection speed gradually increased. This indicated that the burst intensity of the coal samples and the RBL strengthened with increasing strain rate.

3.3.5. Acoustic emission characteristics

The acoustic emission(AE) signals were collected during the loading of coal samples 3–1, 3–2, 3–3, 3–4, 3–5, and 3–7. The loading rates for coal samples, 3–8 and 3–15 were too fast, the AE data were not collected in case the AE sensors were damaged during the

Table 3
Test mechanical parameters of the coal samples during loading at different strain rates.

No.	Loading rate/(mm/min)	Strain rate/s^{-1}	Peak load/kN	*UCS*/MPa	*E*/GPa
1	0.06	9.85E-6	15.37	7.92	1.18
2	0.3	5.18E-5	15.55	7.98	1.31
3	0.6	9.87E-5	17.33	8.88	1.85
4	1.5	2.52E-4	16.23	8.34	1.68
5	3	5.11E-4	22.22	11.33	2.37
6	6	9.81E-4	28.25	14.50	2.51
7	30	5.19E-3	28.80	14.82	2.65
8	60	1.01E-2	81.60	41.90	4.07

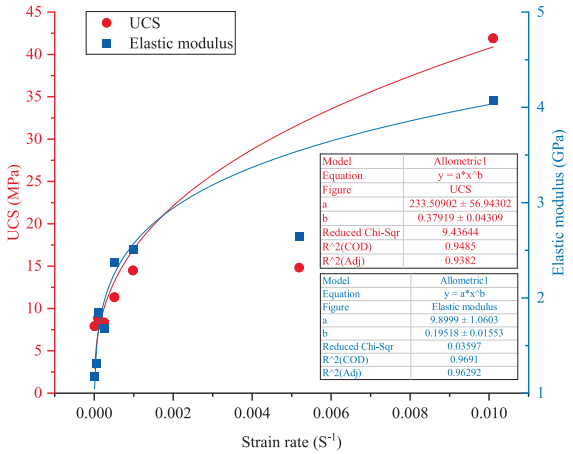

Fig. 7. Correlation between the mechanical parameters and the strain rate.

Table 4
Test results of the parameters of RBL.

No.	Strain rate/s	*UCS* Value/MPa	Classification	K_E Value	Classification	D_T Value/ms	Classification
1	9.85E-6	7.92	Weak	19.79	Strong	19,400	None
2	5.18E-5	7.98	Weak	4.01	Weak	25,000	None
3	9.87E-5	8.88	Weak	17.60	Strong	224	Weak
4	2.52E-4	8.34	Weak	4.50	Weak	6000	None
5	5.11E-4	11.33	Weak	7.02	Strong	780	None
6	9.81E-4	14.50	Strong	4.19	Weak	17	Strong
7	5.19E-3	14.82	Strong	3.71	Weak	44	Strong
8	1.01E-2	41.90	Strong	2.56	Weak	41	Strong

Table 5
Test results of energy input by the press machine.

No.	Strain rate/s	Total/J	Pre-peak/J	Post-peak/J
1	9.85E-6	6.15	5.85	0.30
2	5.18E-5	5.72	4.58	1.14
3	9.87E-5	5.41	5.12	0.29
4	2.52E-4	5.22	4.27	0.95
5	5.11E-4	6.43	5.63	0.80
6	9.81E-4	10.14	8.19	1.95
7	5.19E-3	11.41	8.99	2.42
8	1.01E-2	60.79	43.75	17.06

dynamic failure process.

The corresponding relationship between the AE hit rate and the stress during the loading at different strain rates is illustrated in Fig. 10. The average AE hit rate in the whole loading process is displayed in Fig. 11. It can be seen from Fig. 10 that the stress on the coal samples shows the following trends during the loading process:

(1) All of these samples experienced densification, elastic, yield, failure, and residual strength stages in the loading process.

(2) At a low strain rate, the stress increase was stepped at failure, resulting in the progressive failure of the coal samples. At a high strain rate, the stress curves in the failure stage are steep, therefore coal samples experienced brittle failure.

The following AE signal features can be obtained from Figs. 10 and 11:

(1) In general, the AE hits occurred in the densification stage, the initial section of elastic stage, and the yield failure stage. The AE hit rate in the densification stage was larger than that in the initial section of the elastic stage.
(2) At a low strain rate, the largest AE hit rate was found in the yield failure stage; while as the strain rate increased, the AE hit rate in the densification stage gradually exceeded that in the yield failure stage.
(3) A low AE hit rate in the elastic stage at a low strain rate. While the AE hit rate increased slowly with increasing stress. Moreover, as the strain rate increased, the rate of increase of the AE hit in the elastic stage increased. When the strain rate reached 5.11×10^{-4} s^{-1}, there were blank areas of AE source location in the elastic stage (coal samples 5 and 6).

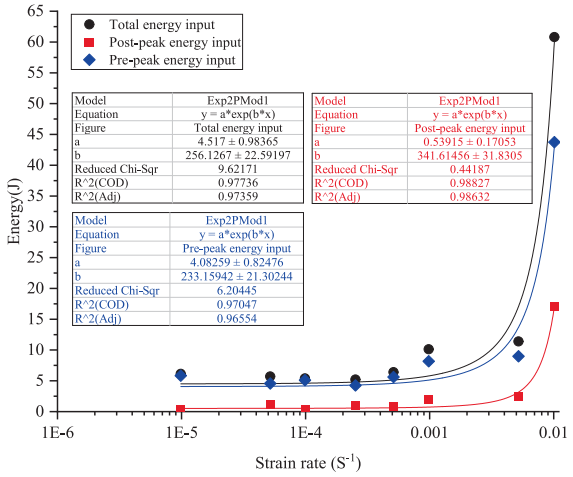

Fig. 8. Energy accumulation and dissipation law with increasing loading strain rate.

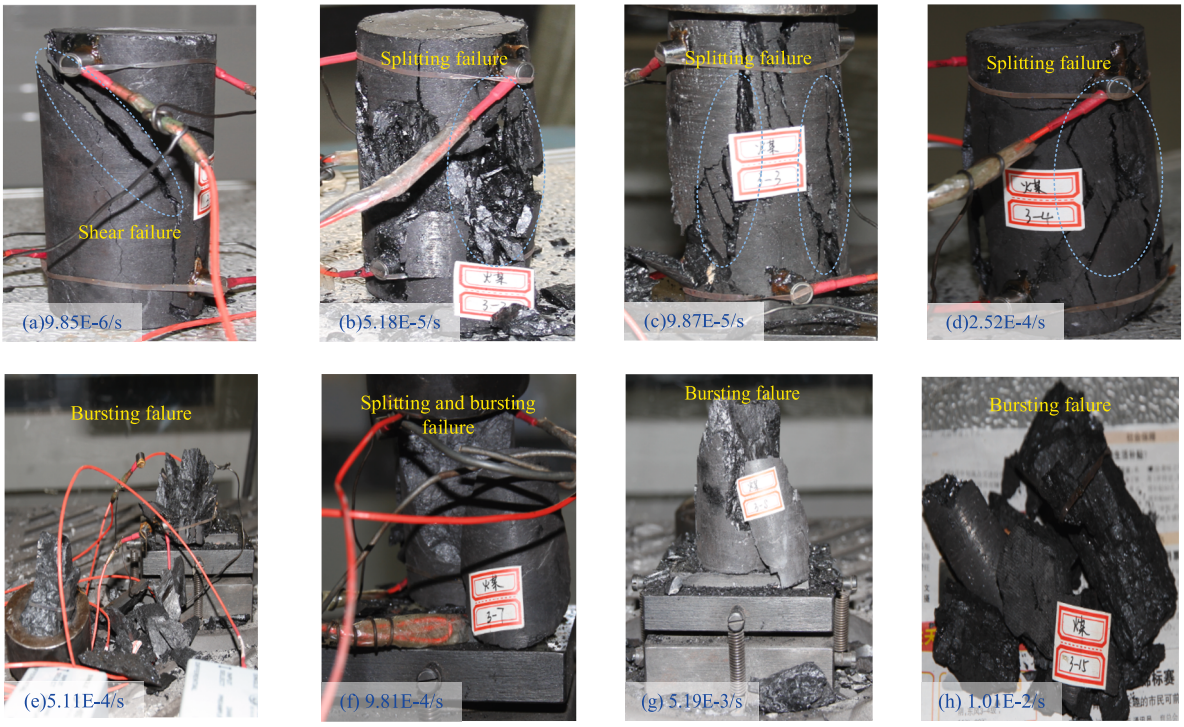

Fig. 9. Correlation between failure mode and loading strain rate.

(4) Although there were blank areas of AE source location for coal samples 5 and 6, the average AE hit rate showed an increasing trend with increasing strain rate.

When the strain rate exceeds 5.11×10^{-4} s^{-1}, a blank area appears in the acoustic emission data. This occurs because the loading speed is too fast, causing the rate of acoustic emission production to reach a critical value. The acoustic emission system could not distinguish between individual acoustic emission events due to the absence of clear time intervals between them. This led to the formation of a continuous acoustic emission waveform, resulting in a blank area in the acoustic emission data. Based on the mechanism behind the blank areas in the acoustic emission data, it can be concluded that the increase in the loading strain rate does not lead to a decrease in the rate of acoustic emission events. Instead, the monitoring anomalies are due to the coal samples breaking too quickly, generating a high number of acoustic emission events at an accelerated rate.

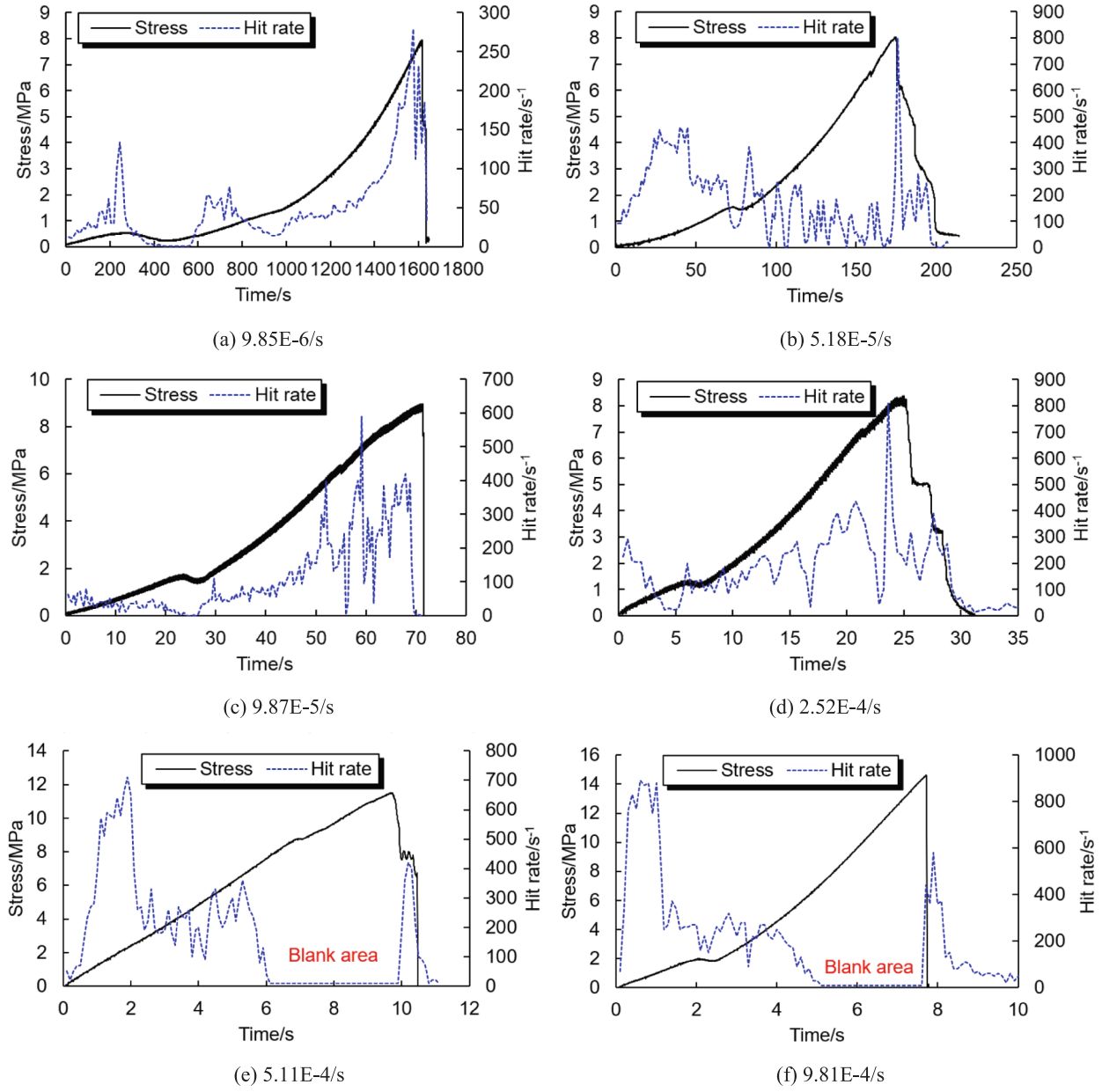

Fig. 10. Relationship between AE hit and stress during loading at different strain rates.

4. Discussion

4.1. Rock burst liability

4.1.1. Energy storage characteristic

With the strain rate increase, the *UCS* and *E* of coal samples both showed an increasing trend subjecting to power function law. According to the formula for calculating the elastic energy of coal rock materials under uniaxial stress conditions [45,46], as shown in Eq. (4).

$$U = \frac{\sigma^2}{2E} \tag{4}$$

Where U is the accumulated elastic deformation energy of coal,σ is stress, and E is elastic modulus. As the *UCS* and *E* of coal show a power function relationship with the loading strain rate, as shown in Fig. 7; According to the analysis of Eq. (4), when σ and E change

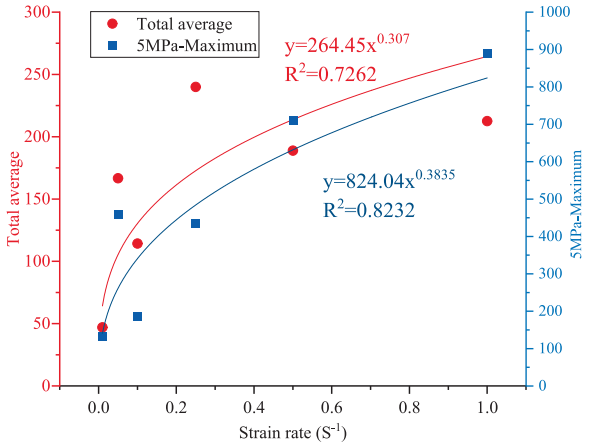

Fig. 11. Relationship between AE hit rate and strain rate.

according to the law of power function, the elastic deformation energy will change according to the law of exponential function, which is consistent with the fitting law of energy accumulation in Section 3.3.3, indicating the reliability of the fitting law. According to Table 3, when the strain rate increases from 5.18×10^{-5} s^{-1}, the static loading increases to 5.19×10^{-3} s^{-1}When subjected to quasi-dynamic loading, the *UCS* and *E* of coal increase by 1.86 and 2.02 times, respectively. Although the increase in *UCS* is slightly smaller than *E*, due to the exponential relationship between elastic energy and stress, the accumulated energy increases by 1.71 times. That is to say, as the loading strain rate increases, the accumulated energy of the coal rock mass under dynamic loading increases. When the loading strain rate reaches 1.01×10^{-2} s^{-1}, the *UCS* and *E* increase by 5.25 and 3.11 times respectively, and the energy increases by 8.86 times at this time, with an extremely fast increase rate. From the analysis of the experimental process, as shown in Fig. 8, the rate of energy input increase after the peak of the coal sample is faster than the rate of energy increase before the peak. This leads to a decrease in the bursting energy index of the coal sample as the loading strain rate increases.

Under dynamic loading, the coal mass undergoes violent and instantaneous brittle failure. During this process, the displacement-controlled testing machine continues to advance at a high strain rate. Consequently, a massive amount of mechanical energy is forcibly dissipated into generating new fracture surfaces, the kinetic energy of ejected fragments, and internal friction. This creates a paradoxical physical phenomenon: although the calculated Bursting Energy Index decreases, the total energy accumulated within the coal sample—as well as the intensity of the failure and the magnitude of energy release—actually increases significantly. Therefore, relying on the traditional static index is fundamentally unsuitable for characterizing the dynamic rock burst liability (RBL) of coal.

4.1.2. Fracture characteristics

From the failure morphology and characteristics of coal samples (Fig. 9), it can be seen that as the loading strain rate increases, the severity of coal failure increases, and the dynamic nature of coal failure increases. Based on the failure characteristics of coal, the RBL of coal increases with the increase of strain rate.

The features of the AE signals indicate that AE hits are closely related to the closure and propagation of cracks in the coal samples. At a low strain rate, there were a few cracks reaching the stress condition for crack propagation at any given time. Therefore, the AE hit rate remained low at low strain rates, while it increased with the strain rate.

The occurrence of the blank areas of AE source location in the elastic stage, seen after the strain rate increased to 5.11×10^{-4} s^{-1}, was mainly because the waveforms of the AE hits were superimposed as the AE hit rate increased to its maximum. In such a context, the AE acquisition instrument failed to distinguish between separate AE hits, finally leading to the appearance of the blank areas of the AE source location. Under these conditions, the coal samples experienced rapid damage and fracturing, accompanied by a high frequency of AE hits. As the strain rate rises, so does the level of AE activity.

Given the observed failure patterns in coal and the insights gained from acoustic emission data, it is evident that the coal's RBL rises as the strain rate increases.

4.1.3. Evolution trend of RBL

Table 4 shows as the strain rate increased, the K_E decreased while the strength of the coal increased. When the coal samples were subject to high stress, the proportion of the energy absorbed during the failure process as deformation energy decreased, such the stress changed only slightly during failure. Therefore, the loading system can still provide sufficient energy to the coal samples in the post-peak phase during the failure process. According to the complete stress–strain curve, the post-peak energy input increased at a faster rate than the pre-peak energy, leading to a reduction in the apparent K_E. Although it might have seemed that the RBL was diminishing, the deformation energy within the coal samples actually increased. Consequently, burst failures were expected to be both more severe and faster. Furthermore, with increasing strain rate, the D_T of the coal samples decreased and the *UCS* increased.

Based on established criteria for evaluating rock burst risk, the risk rises with an increase in strain rate, as supported by all three previously mentioned indicators. In light of this research, it is advisable to use both the total accumulated energy and its rate of change

as metrics for assessing the dynamic RBL of coal under mining-related dynamic loads.To provide a more actionable and rigorous discussion regarding the use of 'total accumulated energy' as an indicator, we propose using the ratio of the total accumulated energy of coal under dynamic strain rate conditions to that under static conditions, rather than relying on absolute energy values, as the specific metric. The bursting energy index is not suitable for this purpose. Instead, the evaluation should incorporate both the dynamic *UCS* and D_T values of the coal to assess its dynamic RBL.

In addition, while the proposed metrics offer a robust assessment under uniaxial conditions, we acknowledge the inherent limitations of this stress path. Deep coal naturally exists in a triaxial stress state. We selected uniaxial testing to simulate the stress-relieved free faces of excavation boundaries where bursts typically trigger, and to ensure a one-to-one comparison with existing national RBL standards. To build upon these findings, conducting true-triaxial dynamic loading tests to investigate the coupled effects of confining pressure and dynamic disturbance will be the primary focus of our future work.

4.2. Rock burst risk under mine tremor dynamic load

The dynamic tests on coal conducted in Chapter 3 demonstrated an enhanced energy accumulation capacity under dynamic loading and revealed the dynamic mechanical response laws of the coal. In the following section, an analysis is presented from the perspectives of fracture mechanics and principal stress rotation to discuss the in-situ mechanical mechanisms by which seismic waves trigger dynamic coal failure and subsequent rock bursts in actual underground mining environments.

4.2.1. Mechanism of dynamic RBL

The failure process of heterogeneous coal rock materials with internal cracks is the result of crack expansion from the perspective of fracture mechanics. From a two-dimensional perspective, the static load state during the actual mining process of coal mines is shown in Fig. 12 as the plane strain state under bidirectional compression. Among them, the crack length is 2 a, the angle between the crack and the principal stress σ_1 is β, and the angle between the crack and the principal stress σ_2 is α.

According to coordinate transformation, the stress field around the crack is:

$$\begin{cases} \sigma_x^{\infty} = -(\sigma_1 \cos^2\beta + \sigma_2 \sin^2\beta) \\ \sigma_y^{\infty} = -(\sigma_1 \sin^2\beta + \sigma_2 \cos^2\beta) \\ \tau_{xy}^{\infty} = -(\sigma_1 - \sigma_2)\sin\beta\cos\beta \end{cases} \tag{5}$$

Where, σ_x^{∞} is normal stress in the x-direction when the crack surface is not affected by size effects, σ_y^{∞} is normal stress on the crack surface in the x-direction, and τ_{xy}^{∞} is shear stress on the crack surface. For coal under pressure, the crack is in a closed state, so the shear force on the crack surface should consider frictional force. At this time, the stress intensity factor of the mode I tensile crack is 0, and the crack is a pure shear crack, that is, a pure mode II crack. At this time, the equivalent shear stress τ_e on the crack surface is:

$$\tau_e = \tau_{xy} - f\sigma_y^{\infty} \tag{6}$$

Where f is the friction coefficient of the crack surface. Then the Stress intensity factor K_{II} is:

$$K_{\mathrm{II}} = (\tau_{xy}^{\infty} - f\sigma_y^{\infty})\sqrt{\pi a} \tag{7}$$

The critical for type II crack propagation is:

$$K_{\mathrm{II}} > K_{\mathrm{IIC}} \tag{8}$$

Where,K_{IIC} is the fracture toughness of coal, which is an inherent parameter of materials. According to the maximum circumferential stress theory [47–49], the critical condition for crack propagation is obtained from Eq. (5) to (8) as follows:

$$\sigma_1 = 2\frac{K_{\mathrm{IIC}}/\sqrt{\pi a} + f\sigma_2}{\sin 2\beta - f(1-\cos 2\beta)} + \sigma_2 \tag{9}$$

The laws governing crack propagation under various stresses and forces will be explored. Utilizing trigonometric functions, Eq. (9) can be transformed into:

$$\begin{cases} \sigma_1 = 2\dfrac{K_{\mathrm{IIC}}/\sqrt{\pi a} + f\sigma_2}{\sqrt{1+f^2}\sin(2\beta+\alpha_f) - f} + \sigma_2 \\ \tan\alpha_f = f \end{cases} \tag{10}$$

When $2\beta + \alpha_f = \pi/2$,$\sigma_1$ has a minimum value:

$$\sigma_{1,\min} = 2\frac{K_{\mathrm{IIC}}/\sqrt{\pi a} + f\sigma_2}{\sqrt{1+f^2} - f} + \sigma_2 \tag{11}$$

Under this situation $\beta = \beta_C = (1/2)\arctan(1/f)$. β_C is the critical angle of crack propagation.

When the denominator of the first part in Eq. (10) is 0, σ_1 takes infinity, and then $\beta = \beta_{\infty 1} = 0$ or $\beta = \beta_{\infty 2} = \arctan(1/f)$. Under this

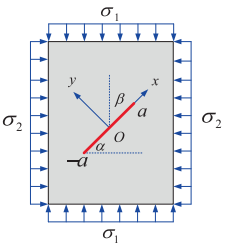

Fig. 12. The stress state of oblique crack beyond extractive space.

situation of $\beta_{\infty 2} < \beta < 90^{\circ}$, the crack could not overcome the friction force to generate crack propagation, and the crack was in a locked state.

Make the relationship between σ_1 and β, as shown in Fig. 13. Analysis shows that when the crack length a and horizontal stress σ_2 are constant, and σ_1 increases to $\sigma_{1,\min}$, the crack that reaches the critical length in the direction β_C first begins to propagate, indicating that crack propagation has an advantageous direction. As the stress further increases to $\sigma_{1,\min} + \triangle\sigma$, cracks near the direction in the range of $\triangle\beta$ begin to propagate, and the greater the increase in stress, the wider the range of crack propagation direction.

According to Eq. (11), when other conditions are constant, crack propagation has a critical length a_C, which is:

$$a_C = \frac{4K_{\mathrm{IIC}}^2}{\pi[(\sigma_1 - \sigma_2)(\sqrt{1+f^2} - f) - 2f\sigma_2]^2} \tag{12}$$

Based on the above analysis, under certain stress conditions, only cracks with a length greater than the critical length near the dominant direction can propagate. That is, under a certain static load, only cracks with a length in the local direction exceeding the critical length can propagate and cause a certain degree of damage to the coal mass. The fracture process is slow, and the coal has fewer fracture surfaces and larger fracture blocks. The amount of acoustic emissions generated during this process is relatively small, and the rate of generation is also relatively low.

4.2.2. Characteristics of rock burst risk under mine tremor dynamic load

From Eqs. (11) and (12), and Fig. 13, it can be seen that in coal mass, only cracks with length exceeding the critical length and a direction near the dominant propagation direction can propagate. By increasing the differential stress between the vertical and horizontal directions can the range of crack propagation direction in the coal rock mass be increased, the critical length of crack propagation be reduced, the number of crack propagation be increased, the degree of damage to the coal rock mass be increased, and thus the probability of coal rock mass failure be increased. Under static load, the stress changes slowly. Therefore, the damage of coal and rock mass under static load only occurs within a small range where the local stress exceeds the critical stress.

When the mine tremor dynamic load acts on the coal mass, the damage and failure under the dynamic static combination are mainly related to the changes in the stress state under the dynamic static combination. Assume that the static load plane principal stress at a particle in the coal mass space is $\boldsymbol{\sigma_s}$, and the dynamic load plane stress varies with time is $\boldsymbol{\sigma_d}$, and the expressions are shown as Eqs. (13) and (14) respectively.

$$\boldsymbol{\sigma_s} = \begin{bmatrix} \sigma_{s1} & 0 \\ 0 & \sigma_{s2} \end{bmatrix} \tag{13}$$

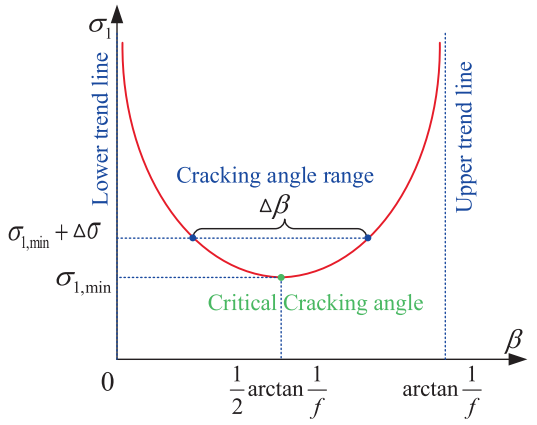

Fig. 13. Relationship between the vertical the stress and oblique crack direction angle.

$$\boldsymbol{\sigma_d} = \begin{bmatrix} \sigma_{d1}(t) & \tau_d(t) \\ \tau_d(t) & \sigma_{d2}(t) \end{bmatrix} \tag{14}$$

Where,σ_{s1} is the first principal stress,σ_{s2} is the second principal stress,$\sigma_{d1}(t)$ and $\sigma_{d2}(t)$ are the time-varying function of normal stress corresponding to dynamic load in two coordinate axis directions,$\tau_d(t)$ is the time-varying function of shear stress generated by the dynamic load.

The combined dynamic and static stress field is:

$$\boldsymbol{\sigma_s} + \boldsymbol{\sigma_d} = \begin{bmatrix} \sigma_{s1} + \sigma_{d1}(t) & \tau_d(t) \\ \tau_d(t) & \sigma_{s2} + \sigma_{d2}(t) \end{bmatrix} \tag{15}$$

The principal stress at this point becomes:

$$\sigma_{p1,p2} = \frac{\sigma_{s1} + \sigma_{s2} + \sigma_{d1}(t) + \sigma_{d2}(t)}{2} \pm \sqrt{\frac{[\sigma_{s1} - \sigma_{s2} + \sigma_{d1}(t) - \sigma_{d2}(t)]^2}{4} + \tau_d(t)^2} \tag{16}$$

The angle of rotation of the principal stress axis relative to the static load is:

$$\theta_p = \frac{1}{2}\arctan\frac{2\tau_d(t)}{\sigma_{s1} - \sigma_{s2} + \sigma_{d1}(t) - \sigma_{d2}(t)} \tag{17}$$

The stress in the coal mass is formed by the combination of dynamic and static loads as shown in Eq. (16). Due to the dynamic load, the combined stress state is a function of time, and the combined stress is in a continuous process of change. Eq. (17) indicates that under dynamic load, the direction of the principal stress continuously rotates and changes over time, and the magnitude of the change is mainly related to the change in dynamic load. These theoretical findings regarding multi-directional crack expansion perfectly corroborate the macroscopic failure modes observed in the field. For instance, the severe roadway closure, roof subsidence, and equipment displacement documented in the 2305S mining face (as previously illustrated in Fig. 3(b)) are direct macroscopic manifestations of this dynamic principal stress rotation mechanism.

The range of dynamic load change is large, and the corresponding range of stress principal axis rotation is also large.As shown in Figs. 14 to 17, based on the raw simulation data from our previous study [50], a new in-depth analysis of the stress field was conducted to investigate the fluctuation patterns of horizontal and vertical stresses at 0.5 m and 5 m from the roadway side under a 1.0×10^6J mining tremor, as well as the rotation pattern of the principal stress axis at these two locations.Analysis shows that the stress in the coal and rock mass can fluctuate greatly during mining tremor, and the direction of the principal stress can vary within a range of 90°. Basically, the principal stress can change in any direction. Therefore, under the action of mining tremors, dynamic loads play a role in changing the magnitude and direction of stress. As shown in Fig. 13, when the magnitude of stress changes, cracks with a larger angle range can reach the critical stress and expand. With the rotation of the stress axis, the dominant direction can rotate accordingly, causing more cracks to expand and damage the coal mass.

The crack length follows a probability distribution due to the presence of a large number of primary and secondary cracks in the coal mass. Under static load, cracks in all directions with a length greater than the critical length of crack propagation in the current static load state in that direction will expand and cause damage to the coal mass. Cracks with a length less than the critical length in that direction will not propagate. When the dynamic load is superimposed, on the one hand, it increases the fluctuation of stress magnitude, reduces the critical length of cracks, and causes more cracks to propagate. On the other hand, it widens the distribution azimuth of the same crack length, even if cracks with a larger range of occurrence propagate.

After dynamic loading, the critical stress for propagation is reduced, due to the large number of crack lengths in the coal mass. At the same time, the damage increases, and the effective stress in the coal rock mass increases, thereby reducing the critical crack length,

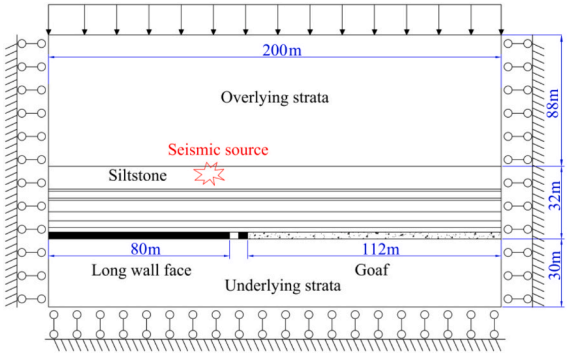

Fig. 14. Model geometry.

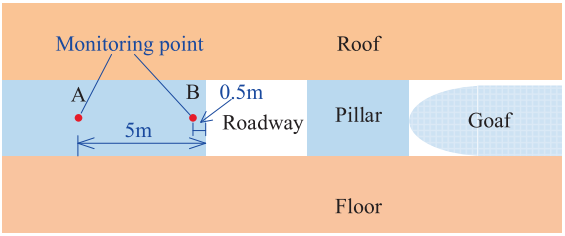

Fig. 15. Settings of monitoring stations.

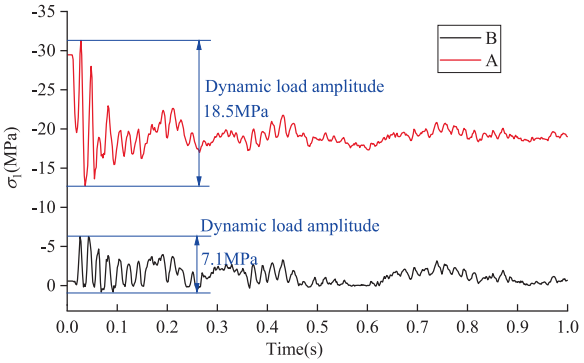

Fig. 16. Stress comparison of 5 m away from coal wall.

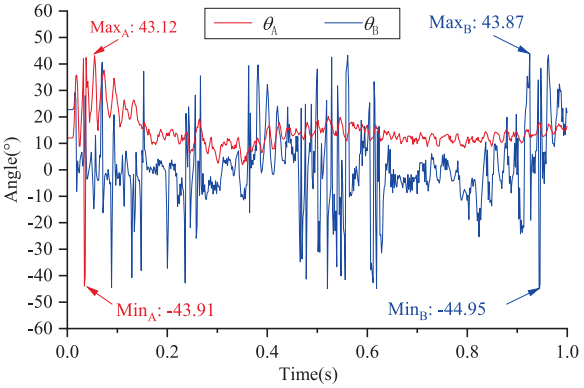

Fig. 17. Changing range of angle between principal stress and axis.

due to the expansion of internal cracks in the coal rock mass. Therefore, after dynamic loading, under pure static loading, the cracks in the coal rock mass will further expand, causing further damage to the coal rock mass. In the process of damage, the stress drop of coal and rock mass decreases. If the system has no external energy input or the stress transfers to the system, the coal and rock system will reach a new equilibrium state. If the coal damage factor reaches the critical damage factor before the system reaches equilibrium, then the coal mass will undergo failure. Therefore, at the moment and after the action of mine tremor vibration load, a large number of cracks dynamically expand in the coal mass in a short time, causing dynamic damage to the coal rock mass and increasing the possibility of losing stability, significantly enhancing the risk of rock burst.

5. Conclusions

In this research, we investigated the mechanics, and RBL, and dynamic fracturing process of coal subjected to similar dynamic load induced by mine tremors. A series of new findings related to the rock burst mechanism have been obtained. The conclusions are as follows:

(1) Field statistics of 474 cases and waveform spectrum analysis confirm that over 83.1% of rock bursts are induced by dynamic disturbances from mine tremors.
(2) As the loading strain rate increases, the energy input to the coal increases exponentially, with post-peak rates exceeding pre-peak rates. This accelerates the transition from static to dynamic failure, accompanied by a surging acoustic emission rate.
(3) Dynamic loading increases the rock burst liability (RBL), evidenced by consistent trends in dynamic UCS and DT. However, the traditional bursting energy index (K_E) paradoxically decreases. Thus, K_E is invalid for dynamic RBL assessment; total energy accumulation and its rate of change should be utilized instead.
(4) Theoretical derivations confirm that coal's energy accumulation relates exponentially to the strain rate, perfectly aligning with experimental results. Consequently, rock burst risk assessments must explicitly account for dynamic tremor disturbances.
(5) Based on fracture mechanics, static loading causes localized crack growth along a dominant direction. In contrast, dynamic loading induces time-varying principal stress rotation, driving instantaneous, multi-directional, and large-scale crack expansion that culminates in violent dynamic failure.

CRediT authorship contribution statement

Jiang He: Writing – review & editing, Methodology, Investigation, Conceptualization. **Guanzhong Qiu:** Writing – review & editing, Writing – original draft, Formal analysis, Data curation. **Linming Dou:** Writing – review & editing, Supervision, Resources, Funding acquisition. **Siyuan Gong:** Writing – review & editing, Methodology, Formal analysis, Conceptualization. **Andrew Pan:** Writing – review & editing, Methodology. **Zonglong Mu:** Writing – review & editing, Validation.

Funding

This work was supported by the State Key Research Development Program of China [grant numbers 2022YFC3004603, 2022YFC3004602]; the Jiangsu Overseas Visiting Scholar Program for University Prominent Young & Middle-aged Teachers and Presidents; the National Natural Science Foundation of China [grant numbers 52227901, 52274147]; and the Natural Science Foundation of Jiangsu Province Basic Research Program [grant number BK20231499].

Declaration of competing interest

The authors declare that they have no known competing financial interests or personal relationships that could have appeared to influence the work reported in this paper.

Acknowledgments

This work was financially supported through grants from the State Key Research Development Programme of China (Grant Nos 2022YFC3004602, 2022YFC3004603), the sponsorship of Jiangsu Overseas Visiting Scholar Program for University Prominent Young & Middle-aged Teachers and Presidents, the National Natural Science Foundation of China (Grant Nos 52227901, 52274147), and the Natural Science Foundation of Jiangsu Province Basic Research Program (Grant No BK20231499). The authors wish to acknowledge these financial contributors and to express their appreciation for the organizations that have supported this research.

Data availability

Data will be made available on request.

References

[1] L.M. Dou, X.Y. Tian, A.Y. Cao, S.Y. Gong, H. He, J. He, W. Cai, X.W. Li, Present situation and problems of coal mine rock burst prevention and control in China, J. China Coal Soc. 47 (1) (2022) 152–171, https://doi.org/10.13225/j.cnki.jccs.yg21.1873 (in Chinese).
[2] M. Bukowska, The rockbursts in the Upper Silesian Coal Basin in Poland, J. Min. Sci. 48 (3) (2012) 445–456, https://doi.org/10.1134/S1062739148030070.
[3] A. Mazaira, P. Konicek, Intense rockburst impacts in deep underground construction and their prevention, Can. Geotech. J. 52 (2015) 1426–1439, https://doi.org/10.1139/cgj-2014-0359.
[4] L.M. Dou, X.Q. He, E.Y. Wang, S.G. Cao, The mechanism of rock burst and seismic waves and its prevention, Ground Press. Strata Control Z1 (1999) 199–203+239 (in Chinese).
[5] L. Yuan, E.Y. Wang, Y.K. Ma, Y.B. Liu, X.L. Li, Research progress of coal and rock dynamic disasters and scientific and technological problems in China, J. China Coal Soc. 48 (5) (2023) 1825–1845, https://doi.org/10.13225/j.cnki.jccs.2023.0264 (in Chinese).
[6] H.E. Lawson, D. Tesarik, M.K. Larson, H. Abraham, Effects of overburden characteristics on dynamic failure in underground coal mining, Int. J. Min. Sci. Technol. 27 (1) (2017) 121–129, https://doi.org/10.1016/j.ijmst.2016.10.001.
[7] C.G. Zhang, I. Canbulata, B. Hebblewhitea, C.R. Wardb, Assessing coal burst phenomena in mining and insights into directions for future research, Int. J. Coal Geol. 179 (5) (2017) 28–44, https://doi.org/10.1016/j.coal.2017.05.011.
[8] Y. Fujii, Y. Ishijma, G. Deguchi, Prediction of coal face rockbursts and microseismicity in deep longwall coal mining, Int. J. Rock Mech. Min. Sci. 34 (1) (1997) 85–96, https://doi.org/10.1016/S1365-1609(97)80035-4.
[9] K. Holub, V. Petroš, Some parameters of rockbursts derived from underground seismological measurements, Tectonophysics 456 (1–2) (2008) 67–73, https://doi.org/10.1016/j.tecto.2006.12.013.
[10] M. Alber, R. Fritschen, M. Bischoff, T. Meier, Rock mechanical investigations of seismic events in a deep longwall coal mine, Int. J. Rock Mech. Min. Sci. 46 (2) (2009) 408–420, https://doi.org/10.1016/j.ijrmms.2008.07.014.

[11] J. He, L.M. Dou, W. Cai, Z.L. Li, Y.L. Ding, Mechanism of dynamic and static combined load inducing rock burst in thin coal seam, J. China Coal Soc. 39 (11) (2014) 2177–2182, https://doi.org/10.13225/j.cnki.jccs.2013.1603 (in Chinese).
[12] L.M. Dou, J. He, A.Y. Cao, S.Y. Gong, W. Cai, Rock burst prevention methods based on theory of dynamic and static combined load induced in coal mine, J. China Coal Soc. 40 (7) (2015) 1469–1476, https://doi.org/10.13225/j.cnki.jccs.2014.1815 (in Chinese).
[13] Y.D. Jiang, Y.X. Zhao, H.W. Wang, J. Zhu, A review of mechanism and prevention technologies of coal bumps in China, J. Rock Mech. Geotech. Eng. 9 (1) (2017) 180–194, https://doi.org/10.1016/j.jrmge.2016.05.008 (in Chinese).
[14] P. Wang, L.S. Jiang, J.Q. Jiang, P.Q. Zheng, W. Li, Strata behaviors and rock burst-inducing mechanism under the coupling effect of a hard, thick stratum and a normal fault, Int. J. Geomech. 18 (2) (2018) 04017135, https://doi.org/10.1061/(ASCE)GM.1943-5622.0001044.
[15] Z.L. Li, L.M. Dou, W. Cai, G.F. Wang, J. He, S.Y. Gong, Y.L. Ding, Investigation and analysis of the rock burst mechanism induced within fault–pillars, Int. J. Rock Mech. Min. Sci. 70 (2014) 192–200, https://doi.org/10.1016/j.ijrmms.2014.03.014.
[16] Z.L. Li, L.M. Dou, W. Cai, G.F. Wang, Y.L. Ding, Y. Kong, Mechanical analysis of static stress within fault-pillars based on a voussoir beam structure, Rock Mech. Rock Eng. 49 (3) (2016) 1097–1105, https://doi.org/10.1007/s00603-015-0754-6.
[17] J. He, L.M. Dou, Gradient principle of horizontal stress inducing rock burst in coal mine, J. Cent. South Univ. 19 (10) (2012) 2926–2932, https://doi.org/10.1007/s11771-012-1360-3.
[18] A.Y. Cao, L.M. Dou, X.X. Bai, Y.Q. Liu, K. Yang, J.Z. Li, C.B. Wang, State-of-the-art occurrence mechanism and hazard control of mine tremors and their challenges in chinese coal mines, J. China Coal Soc. 48 (5) (2023) 1894–1918, https://doi.org/10.13225/j.cnki.jccs.2023.0278 (in Chinese).
[19] S. Wang, A. Cao, C. Wang, W. Guo, C. Xue, J. Liu, X. Wu, G. Shi, Mechanism of rockburst induced by the microseismic event in the floor strata of high tectonic stress zones: a case study, Int. J. Coal Sci. Technol. 11 (1) (2024) 17, https://doi.org/10.1007/s40789-024-00728-3.
[20] T. Li, M.F. Cai, M. Cai, A review of mining-induced seismicity in China, Int. J. Rock Mech. Min. Sci. 44 (2007) 1149–1171, https://doi.org/10.1016/j.ijrmms.2007.06.002.
[21] R.F. Gillian, P.W. Miles, G.G. Jon, R.J. Bruce, J.D. Richard, Global review of human-induced earthquakes, Earth Sci. Rev. 178 (2018) 438–514, https://doi.org/10.1016/j.earscirev.2017.07.008.
[22] J. He, L.M. Dou, S.Y. Gong, J. Li, Z.Q. Ma, Rock burst assessment and prediction by dynamic and static stress analysis based on micro-seismic monitoring, Int. J. Rock Mech. Min. Sci. 93 (2017) 46–53, https://doi.org/10.1016/j.ijrmms.2017.01.005.
[23] W. Cai, X.X. Bai, G.Y. Si, W.Z. Cao, S.Y. Gong, L.M. Dou, A monitoring investigation into rock burst mechanism based on the coupled theory of static and dynamic stresses, Rock Mech. Rock Eng. 53 (12) (2020) 5451–5471, https://doi.org/10.1007/s00603-020-02237-6.
[24] M.C. He, C. Li, W.L. Gong, L.R. Sousa, S.L. Li, Dynamic tests for a constant-resistance-large-deformation bolt using a modified SHTB system, Tunn. Undergr. Space Technol. 64 (2017) 103–116, https://doi.org/10.1016/j.tust.2016.12.007.
[25] J.F. Lou, F.Q. Gao, J.Z. Li, G.Y. Yuan, S. Mostafa, Effect of dynamic loading conditions on the dynamic performance of MP1 energy-absorbing rockbolts: insight from laboratory drop test, Int. J. Min. Sci. Technol. 33 (2) (2023) 215–231, https://doi.org/10.1016/j.ijmst.2022.09.023.
[26] F. Du, J. Ma, X. Guo, T. Wang, X. Dong, J. Li, S. He, D. Nuerjuma, Rockburst mechanism and the law of energy accumulation and release in mining roadway: a case study, Int. J. Coal Sci. Technol. 9 (1) (2022) 21, https://doi.org/10.1007/s40789-022-00521-0.
[27] A. Kidybiński, Bursting liability indices of coal, Int. J. Rock Mech. Min. Sci. Geomech. Abstr. 18 (4) (1981) 295–304, https://doi.org/10.1016/0148-9062(81)91194-3.
[28] GB/T 25217.2–2010. Classification and laboratory test method on bursting liability of coal, Standards Press of China, Beijing, 2010.
[29] T. Szwedzicki, Rock mass behavior prior to failure, Int. J. Rock Mech. Min. Sci. 40 (4) (2003) 573–584, https://doi.org/10.1016/S1365-1609(03)00023-6.
[30] J. He, L.M. Dou, A.Y. Cao, S.Y. Gong, J.W. Lv, Rock burst induced by roof breakage and its prevention, J. Cent. South Univ. 19 (4) (2012) 1086–1091, https://doi.org/10.1007/s11771-012-1113-3.
[31] H. Lan, T.T. Du, Y.W. Peng, C.J. Zhang, Z.H. Qing, Rock-burst mechanism and prevention in working face of shallow buried coal-seam, J. China Coal Soc. 37 (10) (2012) 1618–1623, https://doi.org/10.13225/j.cnki.jccs.2012.10.015, in Chinese.
[32] A.Y. Cao, Y.Q. Liu, F. Chen, Q. Hao, X. Yang, C.B. Wang, X.X. Bai, Focal mechanism and source parameters analysis of mining-induced earthquakes based on relative moment tensor inversion, Int. J. Environ. Res. Public Health 19 (12) (2022) 7352, https://doi.org/10.3390/ijerph19127352.
[33] S. Song, T. Ren, L. Dou, J. Sun, X. Yang, L. Tan, Fracture features of brittle coal under uniaxial and cyclic compression loads, Int. J. Coal Sci. Technol. 10 (1) (2023) 23, https://doi.org/10.1007/s40789-023-00564-x.
[34] J. He, L.M. Dou, W. Cai, Z.L. Li, Y.L. Ding, In situ test study of characteristics of coal mining dynamic load, Shock Vib. 2015 (2015) 121053, https://doi.org/10.1155/2015/121053.
[35] H.P. Xie, J. Lu, C.B. Li, M.H. Li, M.Z. Gao, Experimental study on the mechanical and failure behaviors of deep rock subjected to true triaxial stress: a review, Int. J. Min. Sci. Technol. 32 (5) (2022) 915–950, https://doi.org/10.1016/j.ijmst.2022.05.006.
[36] M. Li, Z.J. Lin, S.L. Shi, D.M. Wang, Y. Lu, H. Li, Q. Ye, X.N. Zhang, Experimental research on influence mechanism of loading rates on rock pressure stimulated currents, Int. J. Min. Sci. Technol. 33 (2) (2023) 243–250, https://doi.org/10.1016/j.ijmst.2022.12.004.
[37] J.C. Wang, F.X. Jiang, X.J. Meng, X.Y. Wang, S.T. Zhu, Y. Feng, Mechanism of rock burst occurrence in specially thick coal seam with rock parting, Rock Mech. Rock Eng. 49 (5) (2016) 1953–1965, https://doi.org/10.1007/s00603-015-0894-8.
[38] S. He, M. Tian, X. He, T. Ren, D. Song, F. Shen, T. Chen, J. Feng, Study on seismic displacement of coal-rock fracture based on radiation energy, Int J Coal Sci Technol 12 (2025) 80, https://doi.org/10.1007/s40789-025-00819-9.
[39] W. Shen, L.M. Dou, H. He, G.A. Zhu, Rock burst assessment in multi-seam mining: a case study, Arab. J. Geosci. 10 (8) (2017) 196, https://doi.org/10.1007/s12517-017-2979-z.
[40] S.N. Glazer. Mine seismology: data analysis and interpretation, Springer International Publishing, Cham, 2016.
[41] C. Zhou, X. He, D. Song, Z. Li, H. Yang, Y. Liu, L. Guo, Study on signal characteristics of burst tendency coal under different loading rates, Int J Coal Sci Technol 11 (2024) 73, https://doi.org/10.1007/s40789-024-00724-7.
[42] W. Cai, L.M. Dou, G.Y. Si, A.Y. Cao, J. He, S. Liu, A principal component analysis/fuzzy comprehensive evaluation model for coal burst liability assessment, Int. J. Rock Mech. Min. Sci. 81 (2016) 62–69, https://doi.org/10.1016/j.ijrmms.2015.09.028.
[43] GB/T 23561.7–2009. Methods for determining the physical and mechanical properties of coal and rock—Part 7: Methods for determining the uniaxial compressive strength and counting softening coefficient, Standards Press of China, Beijing, 2009.
[44] C.Y. Liang, X. Li, S.D. Li, J.M. He, C.F. Ma, Study of strain rates threshold value between static loading and quasi-dynamic loading of rock, Chin. J. Rock Mech. Eng. 31 (6) (2012) 1156–1161 (in Chinese).
[45] H.W. Liu. Material mechanics, Higher Education Press, Beijing, 2004 (in Chinese).
[46] Y. Fu, Y. Wu, J. Li, P. Zhou, Z. Sun, J. He, Mechanical properties and energy evolutions of burst-prone coal samples with holes and fillings, Int J Coal Sci Technol 11 (2024) 40, https://doi.org/10.1007/s40789-024-00675-z.
[47] F. Erdogan, On the crack extension in plates under plane loading and transverse shear, J. Basic Eng. 85 (4) (1963) 519–525, https://doi.org/10.1115/1.3656897.
[48] S.Y. Li, T.M. He, X.C. Yin. Introduction of rock fracture mechanics, Univ. China Sci. Tech. Press, Hefei, 2010.
[49] Z.Y. Cong, Y.W. Li, Y. Liu, Y.H. Xiao, A new method for calculating the direction of fracture propagation by stress numerical search based on the displacement discontinuity method, Comput. Geotech. 140 (2021) 104482, https://doi.org/10.1016/j.compgeo.2021.104482.
[50] J. He, L.M. Dou, Z.L. Mu, A.Y. Cao, S.Y. Gong, Numerical simulation study of hard-thick roof inducing rock burst in coal mine, J. Cent. South Univ. 23 (9) (2016) 2314–2320, https://doi.org/10.1007/s11771-016-3289-4.